nature photonics

ARTICLES

PUBLISHED ONLINE: 6 APRIL 2014 | DOI: 10.1038/NPHOTON.2014.55

The influence of molecular orientation on organic bulk heterojunction solar cells

John R. Tumbleston[1], Brian A. Collins[1†], Liqiang Yang[2], Andrew C. Stuart[2], Eliot Gann[1], Wei Ma[1], Wei You[2]* and Harald Ade[1]*

In bulk heterojunction organic photovoltaics, electron-donating and electron-accepting materials form a distributed network of heterointerfaces in the photoactive layer, where critical photo-physical processes occur. However, little is known about the structural properties of these interfaces due to their complex three-dimensional arrangement and the lack of techniques to measure local order. Here, we report that molecular orientation relative to donor/acceptor heterojunctions is an important parameter in realizing high-performance fullerene-based, bulk heterojunction solar cells. Using resonant soft X-ray scattering, we characterize the degree of molecular orientation, an order parameter that describes face-on (+1) or edge-on (−1) orientations relative to these heterointerfaces. By manipulating the degree of molecular orientation through the choice of molecular chemistry and the characteristics of the processing solvent, we are able to show the importance of this structural parameter on the performance of bulk heterojunction organic photovoltaic devices featuring the electron-donating polymers PNDT–DTBT, PBnDT–DTBT or PBnDT–TAZ.

A power conversion efficiency (PCE) of sunlight to electricity at the 10% level has been achieved in organic photovoltaics (OPVs) based on the bulk heterojunction[1,2] (BHJ) concept. High performance[3,4] has been accomplished using electron-donating polymers and electron-accepting fullerene molecules cast from a common solvent to yield a BHJ thin film (100–250 nm). While simple and potentially inexpensive from a fabrication standpoint, casting from a common solvent leads to a highly complex morphology often classified by domain size, domain purity and aspects of crystallinity (Fig. 1a)[5,6]. Of these morphological characteristics, the extent of polymer crystallization and the average crystallite orientation with respect to the electrodes have been shown to be important factors in many organic electronic devices[7–10] because of the inherent geometric asymmetry of the electronic orbitals of semiconducting polymers. This physical and electronic asymmetry also makes it possible that local polymer orientation near interfaces with electron-accepting fullerenes could be highly relevant to performance. The importance of these interfaces in device functionality is well known, because it is here that critical photo-physical processes such as photo-induced charge separation and recombination take place[11]. However, there is a lack of methods to modify or even characterize preferential orientation relative to donor/acceptor heterointerfaces, which has left this potentially important parameter for achieving high performance unexploited in BHJ devices.

In this Article, we show that polymer orientation relative to donor/acceptor heterointerfaces can preferentially adopt face-on (Fig. 1b) or edge-on (Fig. 1c) orientations in BHJ devices and is a critical parameter for device operation. Using resonant soft X-ray scattering[12], we show that fluorine substitution on the polymer backbone and solvent processing alter the molecular orientation and correlate with device performance. In a polymer where performance does not depend strongly on traditional morphological characteristics[5,6,9,13], we find near-perfect linear correlation between short-circuit current J_{sc} and the degree of molecular orientation (DMO), as well as a high correlation with the fill factor (FF). We further show that this correlation is robust to changes in the polymer chemical moieties, which supports the preliminary conjecture that face-on preferential orientation is an important feature of high-performing BHJ solar cells[14]. Importantly, following observations in bilayer model systems with single planar heterojunctions[15–17], we now show that preferential molecular orientation relative to donor/acceptor heterojunctions is also critical to the ubiquitous fullerene-based BHJ solar cells.

Molecular orientation-performance correlation

We first summarize the impact of variable molecular orientation with respect to donor/acceptor interfaces for blends consisting of the electron-donating polymer poly[naphtho[2,1-*b*:3,4-*b*′] dithiophene–4,7-di(thiophen-2-yl)benzothiadiazole] (PNDT–DTBT)[18]. Two versions of the polymer are used, one with fluorine atoms substituted onto the polymer backbone (red circles in Fig. 1d) and one control with the original hydrogen atoms. Fluorine substitution on the polymer backbone has been noted to improve performance in other BHJ blends[19–21]. Solutions were made by dissolving the polymer and the electron-accepting fullerene phenyl-C_{61}-butyric acid methyl ester (PCBM) (Fig. 1d) in chlorobenzene (CB) or 1,2-dichlorobenzene (DCB) (see Methods for device fabrication). When processed from CB, device performance with the fluorinated blend is slightly enhanced compared to the non-fluorinated control (Fig. 1e). Processing from DCB improves the PCE of the fluorine-based device to 5.6%, but reduces the PCE for the hydrogen-based control to 1.9%. Table 1 shows that differences in performance result primarily from variations in J_{sc} and FF and are not due to variations in optical absorption, as confirmed with optical modelling (Supplementary Fig. 1). Thus, only aspects due to the internal quantum efficiency (that is, the number of charges collected per absorbed photon) are affected.

When plotted against the DMO (determined from the energy-dependent anisotropic scattering signal from polarized soft X-ray scattering; P-SoXS)[12,22], both J_{sc} and FF are strongly correlated

[1]Department of Physics, North Carolina State University, Raleigh, North Carolina 27695, USA, [2]Department of Chemistry, University of North Carolina at Chapel Hill, Chapel Hill, North Carolina 27599, USA; †Present address: National Institute of Standards and Technology, Gaithersburg, Maryland 20899, USA. *e-mail: harald_ade@ncsu.edu; wyou@unc.edu

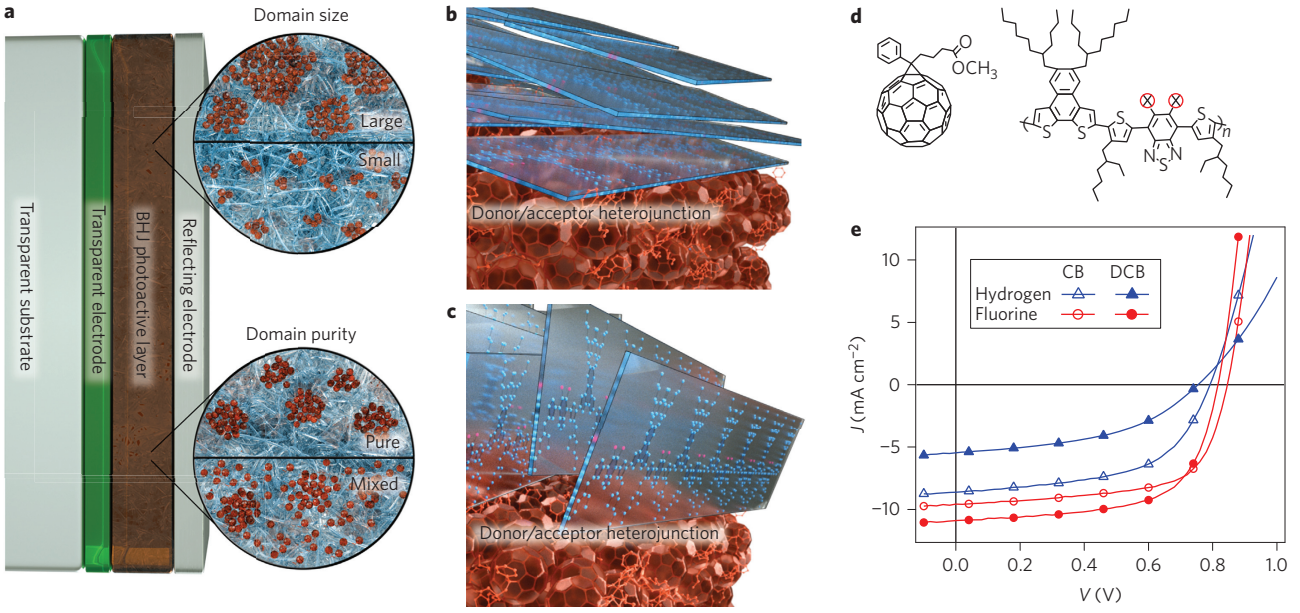

Figure 1 | Device architecture and molecular orientation with respect to donor/acceptor heterojunctions. a, Schematic of a polymer/fullerene BHJ organic solar cell showing device layers as well as zoom-in depictions of the complex morphology of the photoactive layer. Electron-accepting fullerene molecules (dark red) and electron-donating polymer chains (light blue) form domains with different sizes and purities. **b**,**c**, Near donor/acceptor heterojunctions, the polymer can be preferentially oriented in face-on (**b**) or edge-on (**c**) configurations with respect to fullerene domain interfaces. **d**, Chemical structures of fullerene (PCBM) and polymer (PNDT–DTBT) where fluorine is substituted for hydrogen on the polymer backbone (red circles). **e**, Blends based on fluorinated PNDT–DTBT exhibit higher performance than the hydrogen-based controls, with the extent of performance enhancement depending on the choice of processing solvent, either CB or DCB.

Table 1 | Device and morphological parameters.

Polymer	Substituent atoms	Processing solvent	V_{oc} (V) [±0.01]	J_{sc} (mA cm^{-2})	FF (%)	PCE (%)	DMO [±0.03]	Composition variations [±0.1]	Median characteristic length (nm)
PNDT-DTBT	Hydrogen	DCB	0.75	5.5±0.1	46.5±0.4	1.9±0.1	−0.06	0.79	45±4
	Fluorine	DCB	0.81	10.9±0.3	63.6±1.2	5.6±0.2	0.40	1.0	52±6
	Hydrogen	CB	0.79	8.8±0.6	56.1±0.8	3.8±0.2	0.25	0.49	30±3
	Fluorine	CB	0.85	9.6±0.4	64.5±1.3	5.3±0.3	0.29	0.82	112±12
PBnDT-DTBT	Hydrogen	DCB	0.79	11.2±0.5	44.1±0.6	3.9±0.2	−0.04	0.69	28±3
	Fluorine	DCB	0.91	13.0±0.6	54.7±3.5	6.4±0.3	0.31	1.0	43±7
PBnDT-TAZ	Hydrogen	TCB	0.68	10.1±0.6	52.3±2.0	3.6±0.4	0.13	0.87	53±6
	Fluorine	TCB	0.79	12.4±0.5	69.5±2.5	6.8±0.5	0.25	1.0	57±6

PCE is the product of V_{oc}, J_{sc} and FF divided by the incident light intensity (that is, 100 mW cm^{-2}). Composition variations only compare blends based on the same polymer. Characteristic length is derived from the median spatial frequency. Uncertainties for performance parameters correspond to standard deviations of multiple devices, while uncertainties for morphological metrics are estimated from multiple measurements of identical samples.

(Fig. 2a; Pearson's coefficient of $r \geq 0.95$). As discussed in detail in the following, the DMO quantifies the average direction and magnitude of polymer ordering of the polymer-rich domains with respect to the BHJ interfaces. When processed from CB, both polymers demonstrate preferential face-on configurations (positive DMO). When processed from DCB, the fluorinated blend becomes even more strongly face-on, while its non-fluorinated counterpart becomes slightly edge-on (negative DMO). Correspondingly, the device performance of the fluorinated blend improves, but it worsens in the hydrogen-based control. The relationship between DMO and solvent and material choice is probably related to differences in pre-aggregation in the solvent due to differences in backbone and side-chain solubility, as well as different morphological evolution (for example, nodular, fibrillar or fringed micellar) during film-drying after casting.

Although the correlation of DMO with device performance is exceptional, other properties of the morphology, including crystallinity, domain size and domain purity, can play an important role in performance and must be investigated[5,6,9,13,21,23]. In particular, strong π–π stacking of polymer chains is known to assist intermolecular charge transport to the electrodes in many systems[13,24]. In samples of PNDT–DTBT-based blends, grazing incidence wide-angle X-ray scattering (GIWAXS) revealed that π–π stacking is weak, irrespective of atomic substitution or processing solvent (Supplementary Figs 2–4). On the other hand, both the population and size of lamellar crystallites increase dramatically for both blends when processing from DCB rather than CB. However, there is no

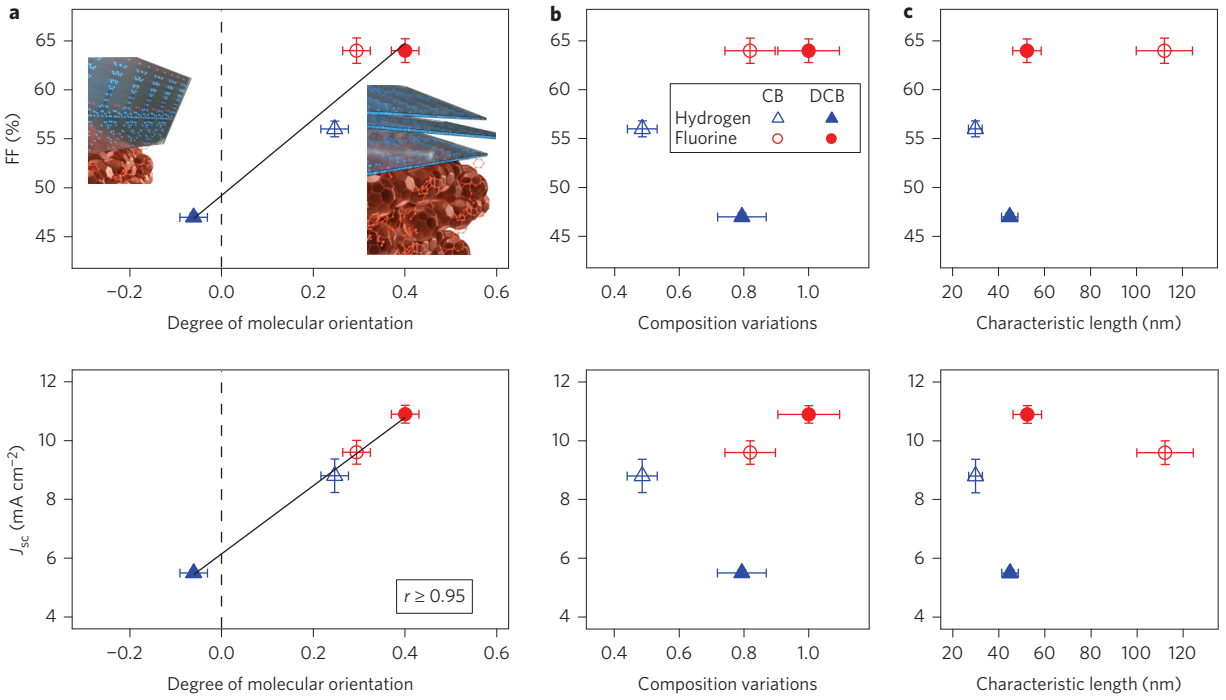

Figure 2 | Device performance strongly correlates with DMO. a–c, FF (top) and J_{sc} (bottom) as a function of DMO (**a**), average composition variations (**b**) and median characteristic length of morphology (**c**) for devices based on PNDT-DTBT polymers that are either fluorinated or hydrogen-based controls. The DMO strongly correlates with FF and J_{sc} (Pearson's $r \geq 0.95$), where positive and negative DMO values correspond to average preferential face-on and edge-on polymer orientations with respect to donor/acceptor heterojunctions, respectively, as depicted schematically in **a**. Perfect face-on and edge-on polymer orientations would correspond to DMO values of +1 and −1, respectively, while DMO = 0 represents random polymer orientation. Best fit lines are also shown in **a**. Uncertainties for performance parameters correspond to standard deviations of multiple devices, while uncertainties for morphological metrics are estimated from multiple measurements of identical samples.

correlation between the performance and these metrics or other metrics related to relative orientation differences of polymer crystallites with respect to the electrodes.

Similarly, poor correlations are found between device performance and the average composition variations measured with P-SoXS, as shown in Fig. 2b (see Supplementary Fig. 5 for details following previous methodology[23]). In short, the mean composition variations within the film are calculated from the total scattering intensity (TSI) and represent relative purity values within a two-phase model, integrated over all size scales corresponding to the measured range of scattering vector **q**. For systems consisting of three phases, the concept of purity is rather complex, yet the composition variation is a model-independent, rigorous parameter that reflects the volume fraction of mixed domains and the dispersion of PCBM. The more dispersed the PCBM, the lower the composition variation. For example, the blend with the largest composition variations—fluorine DCB—has polymer-rich and fullerene-rich domains that have the most compositional contrast. In BHJ solar cells, it is expected that domain purity is an important morphological parameter because Monte Carlo modelling[25] has predicted it to be critical for charge separation and transport. However, in this particular system, even though the composition variations increase for both blends processed from DCB when compared to those processed from CB, paralleling the evolution in crystallinity, performance is improved for the fluorinated blend but is reduced for the hydrogen-based control.

Finally, similarly poor correlations are found between J_{sc} and FF and the spatial frequency distribution that characterizes device morphology. Median characteristic lengths are shown in Fig. 2c and Table 1, with all blends characterized by a narrow distribution of spatial frequencies (Fig. 3c). The median spatial frequency is taken as the q location equal to half the TSI, which is then converted to a median characteristic length via $2\pi/q$. This length is consistent with X-ray and transmission electron microscopy (TEM) measurements (Supplementary Fig. 6). No other characteristic model-free length scale that can be derived from the scattering data[26]—such as the long period (that is, mode), peak or shoulder in $I_{avg}(q)$, the average chord length and so on—correlates with performance.

Because the lack of correlation of individual parameters does not imply they are not important, combinations of parameters have to be considered in order to assess their compensatory, counteracting effects. We start by focusing on the DCB-cast hydrogen-based PNDT–DTBT device using the data in Fig. 2. This device has high crystallinity and small, relatively pure domains, which should lead to good performance within the canonical paradigm, yet it performs the worst. This is contrasted with the fluorine-based DCB device, which performs the best; it has similar crystallinity, but larger domains (which should be detrimental) and only slightly higher purity. Next we compare the CB-cast fluorinated device with the DCB-cast hydrogen-based device which have identical composition variations. Thus, the relative domain compositions are held constant in this comparison. The former device has larger domains and lower crystallinity, both of which should be detrimental, yet it performs significantly better than the latter device. Similar considerations hold when looking at combinations that involve more subtle aspects of crystallinity, such as (100) or (010) coherence length or intensities (Supplementary Fig. 4). Thus, considerations of combinations of parameters other than DMO lead to contradictions in the structure–performance relationships. Ultimately, while generally important, the measured differences in material crystallinity, composition variations and characteristic length scales of the morphology do not strongly determine the FF or J_{sc} of PNDT–DTBT-based blends over the range of changes in these parameters observed here. This indicates that the DMO is a critical morphological

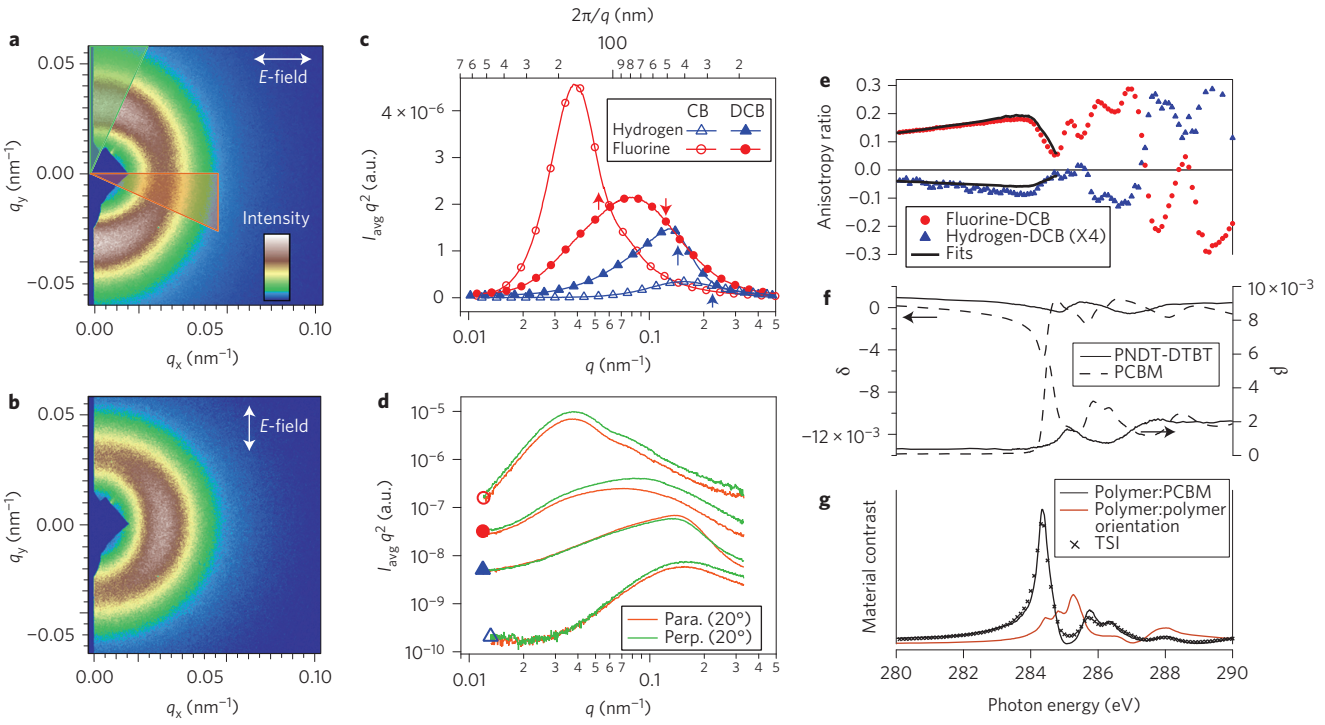

Figure 3 | Polarized soft X-ray scattering anisotropy reveals molecular order. a,**b**, P-SoXS data with horizontally (**a**) and vertically (**b**) linearly polarized X-rays for PNDT-DTBT:PCBM fluorinated blends cast from CB. Greater scattering intensity occurs in the direction perpendicular to the X-ray polarization at this energy. **c**,**d**, Full 180° Lorentz corrected sector averages (**c**) and 20° Lorentz corrected sector averages (**d**) for the wedges shown in **a** for blends with different atomic substitution cast from either CB or DCB. Arrows in **c** correspond to median characteristic lengths, and traces in **d** are vertically offset for clarity. Para., parallel; Perp., perpendicular. **e**, Energy dependence of the anisotropy ratio, $A(E)$, for fluorinated and hydrogen-based blends cast from DCB, as well as model fits to energies below the absorption edge of PNDT-DTBT, which are used to determine DMO as shown in Fig. 2a and Table 1. **f**, The complex indices of refraction ($\tilde{n} = 1 - \delta + i\beta$) for PNDT-DTBT and PCBM constitute the material contrast function ($\Delta\tilde{n}^2$) between polymer and fullerene, which is proportional to $(\Delta\delta)^2 + (\Delta\beta)^2$. **g**, The energy dependence of the TSI matches $\Delta\tilde{n}^2$, indicating that scattering is dominated at virtually all energies by optical contrast between polymer-rich and fullerene-rich domains, not by polymer domains with different orientations. Note: For **c** and **d**, the one-dimensional averaged intensity I_{avg} multiplied by q^2 (that is, $I_{avg}q^2$) corresponds to the Lorentz correction, which is equal to azimuthal integration of our two-dimensional data. This in turn corresponds to the Fourier amplitude of spatial frequencies of a sample.

parameter describing this system and should be investigated when linking performance and morphology in other systems.

Photon energy dependence of anisotropic scattering

The composition variations, characteristic length and DMO shown in Fig. 2 were measured with P-SoXS[12]. As a transmission measurement, P-SoXS measures structures largely in the plane of the BHJ films, with scattering intensity dominated by index of refraction differences between polymer-rich and fullerene-rich regions, and with considerable sensitivity to differences in polymer orientation. The two-dimensional scattering intensity of linearly polarized soft X-rays is shown in Fig. 3a,b for a photon energy of 286.2 eV. Azimuthal integration of the scattering intensity results in reduced data, as shown in Fig. 3c. These traces represent the total intensity for a given $|q|$ and correspond to the distribution of spatial frequencies s in the sample ($|q| = 2\pi s$). Integration is equivalent to 180° azimuthal averages of the intensities (I_{avg}) after application of the Lorentz correction ($I_{avg}q^2$) (ref. 26).

Scattering anisotropy manifests itself in Fig. 3a,b as differing scattering intensities in the directions perpendicular and parallel to X-ray polarization. A very simple, coarse-grained model that provides intuitive understanding of this complex phenomenon is provided in Supplementary Fig. 7. When the polarization is rotated by 90° (Fig. 3b), the higher-intensity scattering lobes also rotate, indicating that the anisotropy indeed originates from local molecular orientational ordering within a globally isotropic film. Because there is scattering in all directions irrespective of the polarization, anisotropic contributions to the scattering are determined by calculating 20° Lorentz-corrected sector averages $I_{avg}(\perp,\parallel)q^2(q)$ perpendicular and parallel to the X-ray electric-field polarization (wedges in Fig. 3a, Fig. 3d). The extent of orientation is quantified by calculating a scattering anisotropy ratio $A(E)$ from the integrated sector intensities $ISI_{(\perp,\parallel)} = \int I_{avg(\perp,\parallel))}q^2(q)\mathrm{d}q$:

$$A(E) \equiv (ISI_{\perp} - ISI_{\parallel})/(ISI_{\perp} + ISI_{\parallel})$$

The materials' feature-rich optical constants near the carbon 1*s* absorption edge give rise to a unique energy dependence of the anisotropy ratio (Fig. 3e), which not only exemplifies the anticorrelated signals of face-on and edge-on orientation for DCB-cast fluorine- and hydrogen-based blends, but is also used to determine the DMO. The DMO (Fig. 2a, Table 1) is obtained from model fits to the energy dependence of the anisotropy ratio using scattering contrast of perfectly aligned polymers with respect to PCBM-rich domains (Fig. 3e; see Supplementary Fig. 8 for an extended discussion). It is an order parameter that measures the average amount of polymer matrix that takes a preferred radial or tangential orientation with respect to PCBM-rich domains. These values range from −1 to +1 for complete polymer edge-on and face-on orientations, respectively, with zero corresponding to random orientation. Even though the DMO is a spatially averaged value, we reason that ordering is probably significant at donor/acceptor interfaces. This assertion is supported by the lack of anisotropic scattering from homopolymer films as would be expected if molecular

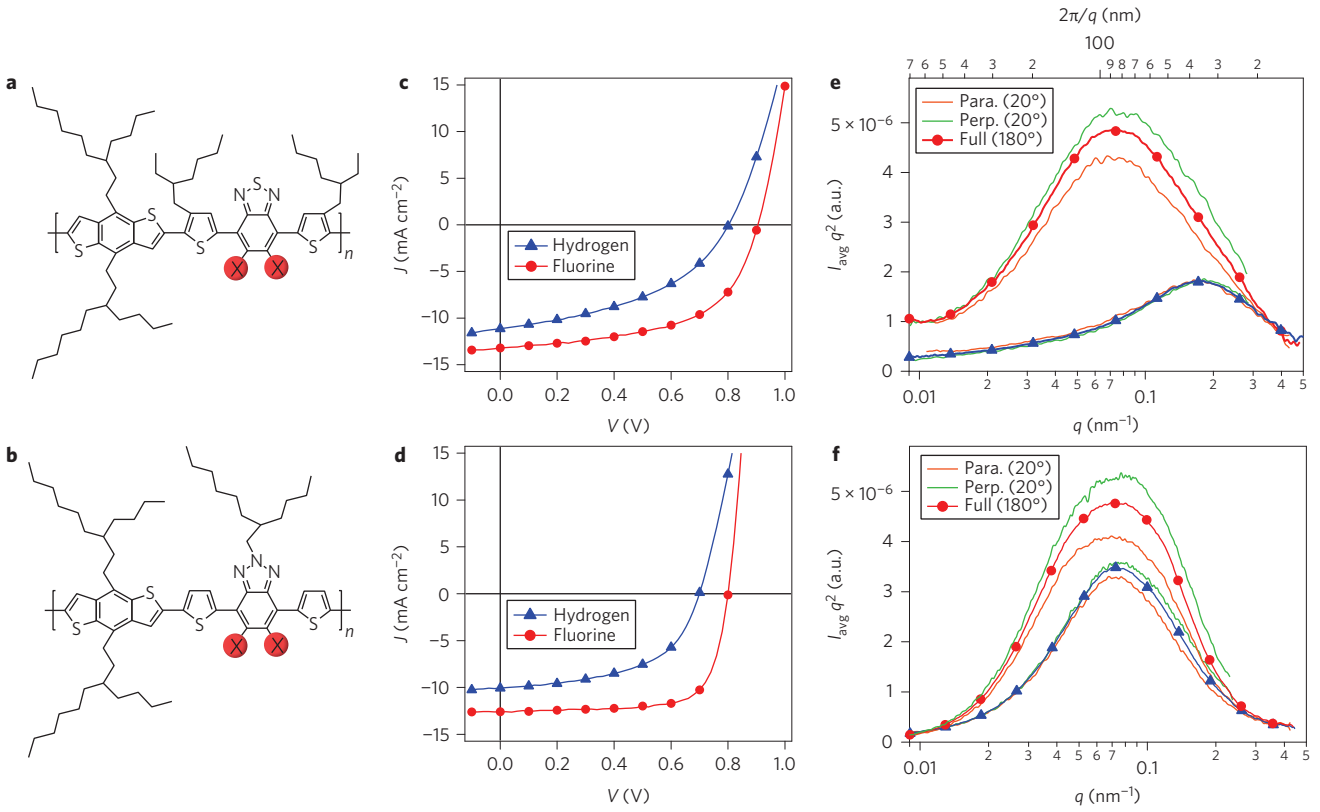

Figure 4 | Face-on molecular orientation correlating to high performance in other systems. a–f, Chemical structures (**a**,**b**), representative device performance (**c**,**d**) and P-SoXS scattering Lorentz corrected sector averages (**e**,**f**) for blends based on PBnDT-DTBT (**a**,**c**,**e**) and PBnDT-TAZ (**b**,**d**,**f**). Face-on molecular orientation and higher performance are observed for blends based on fluorinated versions of both polymers. Slightly edge-on molecular orientation occurs for the hydrogen-based blend of PBnDT-DTBT, while modest face-on orientation occurs for the hydrogen-based control of PBnDT-TAZ. Composition variations and median characteristic lengths are also noted to increase for both fluorinated blends compared to their hydrogen-based counterparts. Horizontally polarized X-rays with photon energies of 284 eV (**e**) and 286.2 eV (**f**) are used to demonstrate the scattering anisotropy in these systems. Para., parallel; Perp., perpendicular.

ordering is randomly nucleated in the middle of polymer-rich domains, for example, from polymer crystallization into fibrillar structures. We note that the correlations of FF and J_{sc} in Fig. 2 with molecular orientation also hold and are meaningful if only the phenomenological $A(E)$ is used.

Together with the energy dependence of the anisotropy ratio, the energy dependence of the TSI, which is a q-integration of full 180° Lorentz-corrected sector averages (Fig. 3c) at each photon energy, eliminates other possible explanations behind the origin of the scattering anisotropy. The contrast functions ($\Delta\tilde{n}^2$) for different scattering sources follow unique energy dependencies set by each material's complex indices of refraction, $\tilde{n} = 1 - \delta + i\beta$ (Fig. 3f). The TSI observed follows the contrast function for material domains of polymer and fullerene and not that of differences in polymer orientation (Fig. 3g), demonstrating that the ordering occurs between polymer-rich and fullerene-rich domains rather than between crystallites or liquid-crystalline ordering within the polymer, as observed in other materials[12]. Likewise, the scattering does not originate from roughness in the film surfaces or voids in the bulk, because the TSI does not match the contrast function for mass-thickness fluctuations (Supplementary Fig. 9). This evidence definitively determines that the anisotropic scattering signal originates from local orientational ordering of the polymer relative to the heterojunction interfaces with fullerene-rich domains.

Generality of face-on molecular orientation and conclusions

Although the DMO has a major influence on the performance of PNDT–DTBT-based devices, demonstrations of structure–property relationships in organic electronics are often confined to one material and cannot be applied universally across material systems. We therefore tested the qualitative correlation of DMO with performance in two other high-performing polymers. When exchanging the NDT moiety of PNDT–DTBT with benzo[1,2-*b*:4,5-*b*′]dithiophene (BnDT), the choice of substituent atom again affects molecular orientation for blends of PBnDT–DTBT[20] (Fig. 4a) and PCBM. Figure 4c,e shows device performance and Lorentz-corrected sector averages from two-dimensional scattering intensity (for example, Fig. 3a) for fluorine-substituted and hydrogen-based control blends processed from DCB. Device performance improves for the fluorine-substituted blends where DMO is positive, indicating a face-on configuration (Table 1). On the other hand, DMO is slightly negative for the hydrogen-based blend. Qualitatively, this is the same result as observed for blends consisting of PNDT–DTBT. Going a step further, when exchanging DTBT with a different moiety, 2-alkyl-benzo[*d*][1,2,3]triazoles (TAZ)[19] (Fig. 4b), fluorination of the backbone again affects the extent of preferential ordering and is correlated to high performance (Fig. 4d,f). This moiety is completely different from DTBT, with the substitution of an additional nitrogen atom and different positioning of the side chain. Through this systematic change in chemical moieties, atomic substitution is revealed to be a general means to enhance performance due to a consistent modification of preferential polymer orientation with respect to donor/acceptor heterojunctions, and is potentially the effect of fluorination.

The effect of improved performance with face-on molecular orientation can be understood with recent developments in device

physics at donor/acceptor interfaces. Specifically, molecular modelling of small-molecule heterojunctions predicts improved electronic coupling due to improved orbital overlap between donor and acceptor materials with face-on orientation. For corresponding solar cell devices with a single planar heterojunction, face-on orientation has been proposed to reduce recombination of photoexcitons during charge separation[16,17]. Also predicted to be mitigated is the recombination of free carriers[15]. Light intensity measurements of PBnDT–TAZ devices indeed reveal that face-on orientation due to fluorine substitution corresponds to a reduction in bimolecular recombination (Supplementary Fig. 10), a key loss mechanism of free carriers in BHJ solar cells[27]. The improved J_{sc} and FF with face-on molecular orientation can therefore be understood by improved exciton dissociation and/or improved charge transport away from heterojunction interfaces due to modifications in the energy landscape at these interfaces[28].

As detailed above, the ability to modify molecular orientation relative to donor/acceptor heterojunctions with atomic substitution is observed for all three different polymer:fullerene-based BHJ devices investigated. Considering also recent small-molecule bilayer results[16,17], molecular face-on ordering relative to donor/acceptor heterojunction interfaces is potentially a general feature of high-performing BHJ organic solar cells. More detailed studies, including the aggregation behaviour in solution, and extensive simulations of the complex interfacial structure[15,29] are required in order to fully clarify the thermodynamic driving forces and kinetics during casting and drying to yield the orientation effects and performance enhancement we report here. Most significantly, interface energetics[28,30,31] and fundamental charge separation and recombination processes[31–33] in fullerene-based BHJ solar cells can now be studied on devices with well-characterized and controlled heterojunctions. Without such controlled interfaces, many measurements cannot be connected directly to theory. Conversely, only a combination of complete characterization and theory constitutes a major step towards the predictive design of high-performing organic solar cells and molecularly designed BHJ interfaces.

Methods

Polymers PNDT–DTBT[18], PBnDT–DTBT[20] and PBnDT–TAZ[19] were synthesized according to previously published methods with the following properties (M_n in kg mol^{-1}; polydispersity): H-PNDT–DTBT (7.62; 2.13), F-PNDT–DTBT (10.5; 2.70), H-PBnDT–DTBT (52.4; 2.0), F-PBnDT–DTBT (39.1; 2.1), H-PBnDT–TAZ (47.6; 2.57), F-PBnDT–TAZ (42.2; 2.36). For solar cells, indium tin oxide (150 nm; 15 $\Omega\square^{-1}$) coated glass substrates were cleaned via sequential sonication in acetone, deionized water and 2-propanol. After ultraviolet-ozone treatment for 30 min, PEDOT:PSS (Baytron PH500) was spun-cast (40 nm) and dried at 140 °C for 10 min. Blends of polymer and PCBM (1:1 wt/wt, 10 mg ml^{-1} for polymers for PNDT–DTBT and PBnDT–DTBT; 1:2 wt/wt, 12 mg ml^{-1} for polymer PBnDT–TAZ) were dissolved in the solvent and heated at 120–140 °C for 6 h. Films based on PNDT–DTBT (~100 nm), PBnDT–DTBT (~150 nm) and PBnDT–TAZ (~250 nm from 1,2,4-trichlorobenzene) were spun-cast on the PEDOT:PSS-coated substrates in a nitrogen glovebox and dried at room temperature in a sealed petri dish for 12 h. Finally, thermal deposition of the cathode (30 nm Ca, 70 nm Al) through a shadow mask resulted in eight devices per substrate (12 mm^2 active area/device). Current density versus voltage (AM 1.5G under 100 mW cm^{-2}) and incident photon to current efficiency measurements were conducted in a nitrogen glovebox using previously described equipment and calibration methods[18–20]. Films for X-ray measurements were cast on PEDOT:PSS-coated Si substrates and processed following the same procedure as devices. P-SoXS measurements were conducted at beamline 11.0.1.2 of the Advanced Light Source (ALS)[22] following previously established methods and protocols[12,18,23] by floating sections of blend films onto silicon nitride windows. GIWAXS was carried out at beamline 7.3.3 of the ALS[34] following previous methods[18] using an incident angle of ~0.12°. Scanning transmission X-ray microscopy was conducted at beamline 5.3.2.2 of the ALS[35] using films floated onto TEM grids. Film thicknesses were measured with profilometry.

Received 19 November 2013; accepted 21 February 2014; published online 6 April 2014

References

1. Halls, J. J. M. *et al.* Efficient photodiodes from interpenetrating polymer networks. *Nature* **376,** 498–500 (1995).
2. Yu, G., Gao, J., Hummelen, J. C., Wudl, F. & Heeger, A. J. Polymer photovoltaic cells—enhanced efficiencies via a network of internal donor–acceptor heterojunctions. *Science* **270,** 1789–1791 (1995).
3. He, Z. *et al.* Enhanced power-conversion efficiency in polymer solar cells using an inverted device structure. *Nature Photon.* **6,** 591–595 (2012).
4. You, J. *et al.* A polymer tandem solar cell with 10.6% power conversion efficiency. *Nature Commun.* **4,** 1446 (2013).
5. Hoppe, H. & Sariciftci, N. S. Morphology of polymer/fullerene bulk heterojunction solar cells. *J. Mater. Chem.* **16,** 45–61 (2006).
6. Chen, L.-M., Hong, Z., Li, G. & Yang, Y. Recent progress in polymer solar cells: manipulation of polymer:fullerene morphology and the formation of efficient inverted polymer solar cells. *Adv. Mater.* **21,** 1434–1449 (2009).
7. Kline, R. J., McGehee, M. D. & Toney, M. F. Highly oriented crystals at the buried interface in polythiophene thin-film transistors. *Nature Mater.* **5,** 222–228 (2006).
8. Salleo, A., Kline, R. J., DeLongchamp, D. M. & Chabinyc, M. L. Microstructural characterization and charge transport in thin films of conjugated polymers. *Adv. Mater.* **22,** 3812–3838 (2010).
9. Rivnay, J., Mannsfeld, S. C. B., Miller, C. E., Salleo, A. & Toney, M. F. Quantitative determination of organic semiconductor microstructure from the molecular to device scale. *Chem. Rev.* **112,** 5488–5519 (2012).
10. Chabinyc, M. L. X-ray scattering from films of semiconducting polymers. *Polym. Rev.* **48,** 463–492 (2008).
11. Graetzel, M., Janssen, R. A. J., Mitzi, D. B. & Sargent, E. H. Materials interface engineering for solution-processed photovoltaics. *Nature* **488,** 304–312 (2012).
12. Collins, B. A. *et al.* Polarized X-ray scattering reveals non-crystalline orientational ordering in organic films. *Nature Mater.* **11,** 536–543 (2012).
13. Brabec, C. J., Heeney, M., McCulloch, I. & Nelson, J. Influence of blend microstructure on bulk heterojunction organic photovoltaic performance. *Chem. Soc. Rev.* **40,** 1185–1199 (2011).
14. Ma, W. *et al.* Domain purity, miscibility, and molecular orientation at donor/acceptor interfaces in high performance organic solar cells: paths to further improvement. *Adv. Energy Mater.* **3,** 864–872 (2013).
15. Verlaak, S. *et al.* Electronic structure and geminate pair energetics at organic–organic interfaces: the case of pentacene/C_{60} heterojunctions. *Adv. Funct. Mater.* **19,** 3809–3814 (2009).
16. Rand, B. P. *et al.* The impact of molecular orientation on the photovoltaic properties of a phthalocyanine/fullerene heterojunction. *Adv. Funct. Mater.* **22,** 2987–2995 (2012).
17. Ojala, A. *et al.* Merocyanine/C_{60} planar heterojunction solar cells: effect of dye orientation on exciton dissociation and solar cell performance. *Adv. Funct. Mater.* **22,** 86–96 (2012).
18. Yang, L., Tumbleston, J. R., Zhou, H., Ade, H. & You, W. Disentangling the impact of side chains and fluorine substituents of conjugated donor polymers on the performance of photovoltaic blends. *Energy Environ. Sci.* **6,** 316–326 (2013).
19. Price, S. C., Stuart, A. C., Yang, L., Zhou, H. & You, W. Fluorine substituted conjugated polymer of medium band gap yields 7% efficiency in polymer–fullerene solar cells. *J. Am. Chem. Soc.* **133,** 4625–4631 (2011).
20. Zhou, H. *et al.* Development of fluorinated nenzothiadiazole as a structural unit for a polymer solar cell of 7% efficiency. *Angew. Chem. Int. Ed.* **50,** 2995–2998 (2011).
21. Albrecht, S. *et al.* Fluorinated copolymer PCPDTBT with enhanced open-circuit voltage and reduced recombination for highly efficient polymer solar cells. *J. Am. Chem. Soc.* **134,** 14932–14944 (2012).
22. Gann, E. *et al.* Soft X-ray scattering facility at the advanced light source with real-time data processing and analysis. *Rev. Sci. Instrum.* **83,** 045110 (2012).
23. Collins, B. A. *et al.* Absolute measurement of domain composition and nanoscale size distribution explains performance in PTB7:PC71BM solar cells. *Adv. Energy Mater.* **3,** 65–74 (2013).
24. Szarko, J. M. *et al.* When function follows form: effects of donor copolymer side chains on film morphology and BHJ solar cell performance. *Adv. Mater.* **22,** 5468–5472 (2010).
25. Lyons, B. P., Clarke, N. & Groves, C. The relative importance of domain size, domain purity and domain interfaces to the performance of bulk-heterojunction organic photovoltaics. *Energy Environ. Sci.* **5,** 7657–7663 (2012).
26. Stribeck, N. *X-Ray Scattering of Soft Matter* (Springer, 2007).
27. Shuttle, C. G., Hamilton, R., O'Regan, B. C., Nelson, J. & Durrant, J. R. Charge-density-based analysis of the current–voltage response of polythiophene/fullerene photovoltaic devices. *Proc. Natl Acad. Sci. USA* **107,** 16448–16452 (2010).
28. Chen, W. *et al.* Molecular orientation dependent energy level alignment at organic−organic heterojunction interfaces. *J. Phys. Chem. C* **113,** 12832–12839 (2009).
29. Beljonne, D. *et al.* Electronic processes at organic–organic interfaces: insight from modeling and implications for opto-electronic devices. *Chem. Mater.* **23,** 591–609 (2010).

30. Vandewal, K. *et al*. Efficient charge generation by relaxed charge-transfer states at organic interfaces. *Nature Mater.* **13,** 63–68 (2014).
31. Albrecht, S. *et al*. On the efficiency of charge transfer state splitting in polymer:fullerene solar cells. *Adv. Mater.* http://dx.doi.org/10.1002/adma.201305283 (2014).
32. Gélinas, S. *et al*. Ultrafast long-range charge separation in organic semiconductor photovoltaic diodes. *Science* **343,** 512–516 (2014).
33. Jailaubekov, A. E. *et al*. Hot charge-transfer excitons set the time limit for charge separation at donor/acceptor interfaces in organic photovoltaics. *Nature Mater.* **12,** 66–73 (2013).
34. Hexemer, A. *et al.* A SAXS/WAXS/GISAXS beamline with multilayer monochromator. *J. Phys. Conf. Ser.* **247,** 012007 (2010).
35. Kilcoyne, A. L. D. *et al*. Interferometer-controlled scanning transmission X-ray microscopes at the Advanced Light Source. *J. Synchrotron Radiat.* **10,** 125–136 (2003).

Acknowledgements

The authors acknowledge the following support for this collaborative research. Characterization and analysis by J.R.T., B.A.C., E.G., W.M. and H.A. was supported by the US Department of Energy (DOE), Office of Science, Basic Energy Science, Division of Materials Science and Engineering under contract DE-FG02-98ER45737. X-ray data were acquired at the ALS, which is supported by the DOE (DE-AC02-05CH1123). W.Y., L.Y. and A.C.S. are supported by the Office of Naval Research (N000141110235) and an NSF CAREER award (DMR-0954280). W.Y. is a Camille Dreyfus Teacher–Scholar. The authors thank D. Kilcoyne at ALS beamline 5.3.2.2, A. Hexemer and S. Alvarez at beamline 7.3.3 and C. Wang and A. Young at beamline 11.0.1.2 for assistance with data acquisition and helpful discussions. F. Liu is thanked for TEM measurements and useful discussions. Insightful discussions with M. Toney (SSRL) are also acknowledged.

Author contributions

J.R.T. and H.A. conceived and designed the experiments. J.R.T. acquired and processed the X-ray data with assistance from B.A.C., E.G., W.M. and H.A. J.R.T., B.A.C. and E.G. conducted X-ray modelling. L.Y. and A.C.S. fabricated and tested devices and prepared all samples. J.R.T., B.A.C. and H.A. wrote the manuscript, with comments and input from all authors. W.Y. and H.A. directed the project.

Additional information

Supplementary information is available in the online version of the paper. Reprints and permissions information is available online at www.nature.com/reprints. Correspondence and requests for materials should be addressed to W.Y. and H.A.

Competing financial interests

The authors declare no competing financial interests.